

UC Berkeley

UC Berkeley Previously Published Works

Title

Formation and Restacking of Disordered Smectite Osmotic Hydrates

Permalink

<https://escholarship.org/uc/item/9z84w795>

Journal

Clays and Clay Minerals, 63(6)

ISSN

0009-8604

Authors

Gilbert, Benjamin
Comolli, Luis R
Tinnacher, Ruth M
[et al.](#)

Publication Date

2015-12-01

DOI

10.1346/ccmn.2015.0630602

Peer reviewed

FORMATION AND RESTACKING OF DISORDERED SMECTITE OSMOTIC HYDRATES

BENJAMIN GILBERT^{1,+}, LUIS R. COMOLLI^{2,+}, RUTH M. TINNACHER¹, MARTIN KUNZ³, AND JILLIAN F. BANFIELD^{4,*}

¹ Earth Sciences Division, Lawrence Berkeley National Laboratory, Berkeley, USA

² Life Sciences Division, Lawrence Berkeley National Laboratory, Berkeley, USA

³ Advanced Light Source, Lawrence Berkeley National Laboratory, Berkeley, USA

⁴ Earth and Planetary Sciences, University of California – Berkeley, Berkeley, USA

Abstract—Clay swelling, an important phenomenon in natural systems, can dramatically affect the properties of soils and sediments. Of particular interest in low-salinity, saturated systems are osmotic hydrates, forms of smectite in which the layer separation greatly exceeds the thickness of a single smectite layer due to the intercalation of water. *In situ* X-ray diffraction (XRD) studies have shown a strong link between ionic strength and average interlayer spacing in osmotic hydrates but also indicate the presence of structural disorder that has not been fully described. In the present study the structural state of expanded smectite in sodium chloride solutions was investigated by combining very low electron dose, high-resolution cryogenic-transmission electron microscopy observations with XRD experiments. Wyoming smectite (SWy-2) was embedded in vitreous ice to evaluate clay structure *in aqua*. Lattice-fringe images showed that smectite equilibrated in aqueous, low-ionic-strength solutions, exists as individual smectite layers, osmotic hydrates composed of parallel layers, as well as disordered layer conformations. No evidence was found here for edge-to-sheet attractions, but significant variability in interlayer spacing was observed. Whether this variation could be explained by a dependence of the magnitude of long-range cohesive (van der Waals) forces on the number of layers in a smectite particle was investigated here. Calculations of the Hamaker constant for layer-layer interactions showed that van der Waals forces may span at least five layers plus the intervening water and confirmed that forces vary with layer number. Drying of the disordered osmotic hydrates induced re-aggregation of the smectite to form particles that exhibited coherent scattering domains. Clay disaggregation and restacking may be considered as an example of oriented attachment, with the unusual distinction that it may be cycled repeatedly by changing solution conditions.

Key Words—Clay Swelling, Cryogenic Transmission Electron Microscopy, Montmorillonite, van der Waals Forces.

INTRODUCTION

Despite their widespread importance in soils, sediments, oceans, the atmosphere, and for technological applications, scientific understanding of the behavior of swelling clays, such as smectite, is incomplete (Low and Margheim, 1979; Laird, 2006). Clay swelling influences significantly the structure and permeability of soils and subsurface sediments including clay-rich shales (Anderson *et al.*, 2010). Smectite comprises a variety of 2:1 layer silicates with sufficiently low charge to enable them to swell, accommodating water molecules and organic compounds in the interlayer region (Foster, 1955; Laird, 2006). At elevated temperature and very dry conditions, all interlayer water may be removed. In humid air or high-ionic-strength solutions, smectites can accommodate between 1 and 3 ordered layers of water, forming “crystalline hydrates” with basal spacings that

vary in discrete steps from 1.1 to 1.9 nm (Dazas *et al.* 2015).

In low-ionic-strength solutions, smectites can incorporate a much larger amount of water into the interlayer region than would be the case for high-ionic-strength solutions. In this regime, expansion of the clay is driven by an osmotic process (Norrish, 1954) justifying the description of the consequent structured material as “osmotic hydrates” (*cf.* Luckham and Rossi, 1999). In a landmark paper, Norrish (1954) reported that smectite undergoes a discontinuous (first-order) transition from the crystalline to osmotic hydrate state as solution ionic strength is decreased. At concentrations of $< \sim 0.25$ M NaCl for Wyoming bentonite, the separation between layers shows a linear dependence on $N^{-1/2}$, where N is the salt concentration. Remarkably, this trend was observed out to periodicities of ~ 14 nm and was subsequently shown to be a function of salt type and concentration, clay concentration and layer charge, and temperature (Viani *et al.*, 1983; Slade *et al.*, 1991; Zhang *et al.*, 1993; Faisandier *et al.*, 1998; Amorim *et al.*, 2007; Svensson and Hansen, 2013).

* E-mail address of corresponding author: jbanfield@berkeley.edu

⁺ Equal co-authors

DOI:

1 In osmotic hydrates, equilibrium layer-layer separa- 1
2 tions derive from a competition between repulsive 2
3 electrostatic forces and attractive van der Waals (vdW) 3
4 forces between the layers (Laird, 2006). Because both 4
5 interactions are reduced by the shielding effect of 5
6 interlayer ions, the interlayer spacing exhibits the 6
7 observed dependence on ionic strength. The same 7
8 concepts underpin the theory of colloid dispersions 8
9 predicted by the theory of Derjaguin and Landau, 9
10 Verwey and Overbeek (DLVO), and hence many 10
11 treatments of this regime apply DLVO theory 11
12 (Greathouse *et al.*, 1994; Liu, 2013). For smectite with 12
13 low structural charge (such as montmorillonite) and 13
14 monovalent ions, these approaches can reproduce trends 14
15 in interlayer spacing with ionic strength. For example, 15
16 Quirk and Marčelja (1997) showed DLVO theory to 16
17 correctly predict the interlayer separation of Li-mont- 17
18 morillonite from 1.8 to 12 nm as a function of pressure 18
19 and LiCl concentration. DLVO failed, however, to 19
20 predict accurately the ionic-strength threshold for 20
21 aggregation (Missana and Adell, 2000) and swelling 21
22 pressure (Viani *et al.*, 1983). Moreover, all models based 22
23 on DLVO theory fail to depict accurately behavior for 23
24 highly charged surfaces or non-monovalent ions such as 24
25 Ca^{2+} (Kleijn and Oster, 1982). 25

26 All XRD and small-angle X-ray scattering (SAXS) 26
27 studies of smectite osmotic hydrates show evidence of 27
28 disorder in the interlayer spacings (Quirk and Marčelja, 28
29 1997; Faisandier *et al.*, 1998). Whether this is caused by 29
30 intrinsic heterogeneity of natural smectites, with cation 30
31 substitutions leading to local variations in layer charge or 31
32 whether it is simply a consequence of natural fluctuations 32
33 due to, *e.g.* Brownian motion, is not known. Molecular 33
34 simulations have predicted that alternative stacking 34
35 configurations, such as edge-to-face, could prevail under 35
36 certain conditions (Jönsson *et al.*, 2008). Tests of such 36
37 predictions are currently lacking, however. 37

38 The present authors suggest that osmotic hydrates 38
39 contain structural disorder that has not been fully 39
40 characterized by any prior study and that a better 40
41 understanding of this disorder would advance knowledge 41
42 of the forces between clay layers. Conventional methods 42
43 are unable to reveal detailed information about hydrated 43
44 smectite structure. Despite recent advances in the 44
45 analysis of X-ray scattering data, this approach has 45
46 limited the ability to characterize disorder in suspensions 46
47 of anisotropic crystallites. Accurately quantifying the 47
48 distributions of different layer hydration states in 48
49 crystalline hydrates is possible from XRD data (Pons 49
50 *et al.*, 1981; Ferrage *et al.*, 2005; Dazas *et al.*, 2015), but 50
51 not the distributions of spacings in osmotic hydrates. 51
52 Even fewer attempts have been made to quantify 52
53 disorder in osmotic hydrates. Several groups have used 53
54 SAXS to explore the average distances between layers in 54
55 completely exfoliated smectite as a function of solution 55
56 conditions (*e.g.* Paineau *et al.*, 2011). Interpretation of 56
57 SAXS data beyond quantification of mean interlayer 57

1 spacings is very model dependent, however, and direct 1
2 observations of layer disorder, useful for validating 2
3 proposed models, have not been reported to date. 3

4 Only transmission electron microscopy (TEM) has 4
5 the necessary spatial resolution for imaging smectite 5
6 particles. Guthrie and Veblen (1989) showed that it was 6
7 possible to measure coherent stacking sequences in 7
8 mixed-layer illite-smectite. The ultrahigh vacuum condi- 8
9 tions required for TEM can cause complete loss of 9
10 interlayer water, however. Many groups have studied 10
11 smectites that were expanded by alkylammonium inter- 11
12 calation and preserved in epoxy (*e.g.* Schumann *et al.*, 12
13 2014) but epoxy intrusion into the interlayers can alter 13
14 interlayer spacing relative to values observed by XRD 14
15 for hydrated systems. These conventional TEM methods 15
16 are even less suitable for studying osmotic hydrates. 16

17 Here a first imaging study of smectite in the osmotic 17
18 hydrate state using cryogenic transmission electron 18
19 microscopy (cryo-TEM) is reported. Rapid vitrification 19
20 of samples enabled electron microscopy imaging of 20
21 particles in aqueous suspensions. The flash freezing 21
22 approach has been proven to preserve the structure of 22
23 hydrated biological macromolecules such as ribosomes 23
24 for which independent atomic-resolution structures exist 24
25 (see Cheng, 2015, and references therein). Cryo-TEM 25
26 has previously been used to determine the structure of 26
27 microbial mineral precipitates (Comolli *et al.*, 2011) and 27
28 the structure of fragile, extended aggregates of Fe 28
29 oxyhydroxide nanoparticles (Yuwono *et al.*, 2010; 29
30 Frandsen *et al.*, 2014; Legg *et al.*, 2014). Cryo-TEM 30
31 was used by Segad *et al.* (2012) to compare the 31
32 aggregate structures of Na- and Ca-equilibrated mont- 32
33 morillonite suspensions, but without investigating the 33
34 osmotic hydrate regime. 34

35 In the current study a state-of-the-art low-dose cryo- 35
36 TEM was used to characterize osmotic hydrates formed 36
37 by a montmorillonite from a Wyoming bentonite 37
38 (SWy-2). The bentonite was either studied without 38
39 treatment, or was treated with standard methods to 39
40 obtain a purified, Na-equilibrated montmorillonite frac- 40
41 tion of sub-2 μm particles. Image details led the authors 41
42 to speculate that variations in interlayer spacings arise 42
43 neither from intrinsic layer charge heterogeneity nor 43
44 from random Brownian motion, but rather from the 44
45 action of vdW forces which extend over multiple 45
46 interlayer distances. This length scale is not typically 46
47 considered in theories of smectite swelling. Because 47
48 configurational disorder prevented direct validation of 48
49 this concept in the present study, the idea was tested 49
50 using a recently developed computational method for 50
51 prediction of vdW forces in multi-layer geometries. 51
52 Despite lack of the materials-properties data required for 52
53 accurate predictions for layered aluminosilicates in high- 53
54 salinity solutions, calculations in the present study 54
55 suggest strongly that equilibrium interlayer spacings in 55
56 osmotic hydrates are influenced by layer-layer vdW 56
57 forces that extend across multiple smectite layers. 57

MATERIALS AND METHODS

Experimental methods

Clay treatments. The experiments used samples of the Source Clay SWy-2 from the Source Clays Repository of The Clay Minerals Society (<http://www.clays.org/SOURCE%20CLAYS/SCBackground.html>). SWy-2 is a Na-rich bentonite from Crook County, Wyoming, in which the smectite fraction is montmorillonite. A multistep treatment of this material was performed to create a homoionic Na-saturated suspension free of mineral impurities referred to as Na-montmorillonite. The steps are described in more detail in the Supplementary Information section (deposited with the Editor in Chief and available at <http://www.clays.org/JOURNAL/JournalDeposits.html>), and included (1) the removal of calcite impurities using a 1 M sodium acetate/0.564 M glacial acetic acid solution, (2) the equilibration of the clay with a 1 M sodium chloride solution, (3) the removal of excess Na-salts with Nanopure water, (4) the separation of quartz and feldspar impurities from clay particles by centrifugation while retaining the <2 μm fraction, and (5) oven-drying of the purified clay mineral phase at 45°C (~2 weeks). Steps 1–3 were performed by dialysis. The dried clay was recovered and ball milled for 2 min and stored dry until its resuspension in NaCl solutions.

Dried smectite was pressed into powder pellets, carbon coated, and analyzed by electron probe microanalysis (EPMA) with a Cameca SX-51 in the Department of Earth and Planetary Science at the University of California, Berkeley, USA. Data acquisition, analysis, and correction procedures were conducted with the software, *Probe*, for EPMA, as described in the Supplementary Information section.

Cryo-TEM specimen preparation and instrumentation.

As-received or treated samples of dried and powdered Wyoming montmorillonite were suspended in water or NaCl solutions at salt concentrations below the crystalline-to-osmotic transition threshold (~0.25 M). Samples were equilibrated overnight. Aliquots of 5 μL were taken directly from the suspensions, placed onto 200 mesh lacey carbon formvar or 300 mesh lacey carbon Cu-grids (Ted Pella, Incorporated, California, USA, #01881 and #01895, respectively), manually blotted with filter paper and plunged into liquid ethane at liquid nitrogen temperature. The TEM grids had previously been glow discharged.

Images were acquired on a JEOL-3100-FFC electron microscope equipped with a field emission gun (FEG) electron source operating at 300 kV, an Omega energy filter, and a cryo-transfer stage. Images were recorded on a Gatan 795 4k \times 4k charge-coupled device (CCD) camera (Gatan Inc., Pleasanton, California, USA) mounted at the exit of an electron decelerator operated at 200 kV, resulting in images formed by a 100 kV electron beam

at the CCD. The stage was cooled to 80 K with liquid nitrogen during the acquisition of all data sets.

Cryo-TEM image acquisition and analysis. Over 100 two-dimensional (2D) images were recorded at nominal magnifications of 50 k \times , 80 k \times , 120 k \times , and 200 k \times giving pixel sizes of 0.112 nm, 0.07 nm, 0.047 nm, and 0.028 nm at the specimen, respectively. Underfocus values ranged between $\sim 1000 \pm 100$ nm and 35 ± 5 nm (measured from minimum contrast), and energy filter widths were typically ~ 30 eV. The survey of the grids and the selection of suitable targets were done in low-dose defocused diffraction mode to minimize radiation damage, as established for biological samples (Luef *et al.*, 2012). Images were acquired under low-dose conditions, typically with doses of ~ 125 –250, 320, 720, and 1000 $\text{e}^- \text{\AA}^{-2}$ per image for nominal magnifications of 50 k \times , 80 k \times , 120 k \times , and 200 k \times . The software *ImageJ* 1.38x, National Institutes of Health (NIH) (<http://rsb.info.nih.gov/ij/>) was used for analysis and measurements of the 2D image projections.

X-ray diffraction. Powdered samples of treated SWy-2 were suspended in NaCl solutions or ultrapure water at a smectite concentration of 200 $\mu\text{g}/\text{mL}$ for 1 week. A small aliquot of the suspensions was placed in 300- μm internal-diameter quartz capillaries for synchrotron XRD analysis at beamline 12.3.2 at the Advanced Light Source. For improved powder statistics, samples within the capillary were scanned over a 100 $\mu\text{m} \times 100 \mu\text{m}$ (5 μm steps) area through a 2 \times 10 μm 10 keV beam, equivalent to a wavelength of 1.2398 \AA . Powder patterns were recorded in 600-s exposures using a Pilatus-1M area detector (Dectris, Baden-Dättwil, Switzerland) positioned at 20°2 θ and ~ 190 mm distance. The experimental geometry was calibrated using Al₂O₃ National Institutes of Standards and Technology (NIST) standard material (SRM 676a). Initial suspensions were too dilute to provide either interlayer or in-plane diffraction peaks, so the capillaries were spun at 10 krpm for 2 h in a special insert machined to fit an Eppendorf centrifuge. Centrifugation caused a visible increase of clay density in the salt suspension and permitted analysis by XRD. A portion of the same sample was dried on a filter, removed gently and re-powdered, and placed into an identical capillary. The low-angle (1.8–8°2 θ) data were processed by fitting and removing an exponential function corresponding to scattering from water. The wide-angle (5–35°2 θ) data were processed by subtracting the scattering from an empty capillary.

Calculations

Van der Waals force calculation. The freely available *Gecko Hamaker* code (Rajter *et al.* 2013) was used for simulating the vdW interactions within multi-layered models of stacked smectite in water. The *Gecko* code calculates the Hamaker constant A_{123} for the interaction

1 between two structured objects 1 and 3 separated by
 2 medium 2 of thickness D . The approach was described
 3 fully by Podgornik and Parsegian (2004) and Parsegian
 4 (2006) and is based upon the theory of Lifshitz (1956)
 5 that links the complex optical properties of two solids to
 6 the dispersion forces between them. The vdW force per
 7 unit area, P_{vdW} , is then calculated from:

$$P_{\text{vdW}} = \frac{A}{6\pi D^3}$$

8
 9
 10
 11 A series of calculations was designed to test the
 12 hypothesis that long-range vdW interactions (beyond
 13 next nearest neighbor layers) made a significant
 14 contribution to the overall cohesion energy of a smectite
 15 particle with a uniform interlayer spacing that was fixed
 16 at either 4 or 5 nm. Given the lack of optical-property
 17 measurements for layer silicates, a silica-corundum-
 18 silica stack was used to approximate one individual 2:1
 19 layer, using material constants for corundum (Al_2O_3)
 20 and amorphous silica (SiO_2) from the *Gecko* database
 21 (French *et al.* 1998; Tan *et al.* 2005). A full calculation
 22 of clay particle cohesion energy as a function of all
 23 relevant parameters will require new dielectric measure-
 24 ments for layer silicates and for salt solutions.

25 The Hamaker constant for inner- and outermost pairs
 26 of clay layers was calculated as a function of the total
 27 number of layers in a clay particle, from 2 to 14. For
 28 these calculations the intervening solution was pure water
 29 because the dielectric functions for electrolyte
 30 solutions are not known accurately. A portion of the
 31 vdW forces are effectively screened by electrolyte
 32 solutions, but the most significant part involves electro-
 33 nic fluctuations which occur on a timescale that is far too
 34 short to be effectively screened by the motion of ions in
 35 solution (Davies and Ninham, 1972). No previous study
 36 of ionic-strength effects on vdW interactions between
 37 minerals could be found by the present authors.
 38 However, Marra (1985) showed that the strength of
 39 vdW interactions between digalactosyl-diglyceride
 40 bilayers decreased by ~50% in 0.2 M NaCl compared
 41 to water. Therefore, the 0.1 M solution used in the
 42 present study was assumed to reduce the vdW strength
 43 by half relative to that predicted for pure water. This
 44 correction factor was not applied to the calculations.
 45

46 *Electrostatic force calculation.* For comparison with the
 47 magnitude of the vdW interaction forces, the electro-
 48 static repulsion pressure between two model ‘mont-
 49 morillonite’ layers in 0.1 M NaCl was calculated. The
 50 pressure, P_{EDL} , was calculated from the force between
 51 overlapping electrical double layers (EDL):

$$P_{\text{EDL}} = \frac{1}{2} \epsilon_r \epsilon_0 \kappa^2 \Phi_0^2 \left(\frac{1}{\cosh \frac{\kappa D}{2}} \right)^2$$

52
 53
 54
 55
 56
 57 where $\kappa = (\epsilon_r \epsilon_0 R T / 2 z^2 F^2 c)^{1/2}$ is the inverse Debye length,
 $\epsilon_r \epsilon_0$ is the dielectric permittivity of water, R is the ideal

1 gas constant, $T = 298$ K is temperature, $z = 1$ is the ionic
 2 valence, Φ is Faraday’s constant, and c is the bulk
 3 electrolyte concentration (in ions/cm³). The surface
 4 potential, Φ_0 , was fixed at 250 mV (Miller and Low,
 5 1990; Hou *et al.* 2009).

RESULTS

6
 7
 8
 9 Both intact and treated SWy-2 formed visually clear
 10 suspensions readily after equilibration in 0.1 M NaCl
 11 solution at smectite concentrations of 50 µg/mL or
 12 lower. Representative low-magnification defocused dif-
 13 fraction imaging of cryo-TEM preparations are shown in
 14 Figures S1–S3 (deposited with the Editor in Chief and
 15 available at [http://www.clays.org/JOURNAL/](http://www.clays.org/JOURNAL/JournalDeposits.html)
 16 [JournalDeposits.html](http://www.clays.org/JOURNAL/JournalDeposits.html)). The suspensions contained a
 17 dispersion of individual layers consisting of one
 18 octahedral and two tetrahedral sheets (2:1 layers), the
 19 fundamental structural unit of smectite, and particles
 20 containing multiple stacked 2:1 layers (smectite parti-
 21 cles). Higher-magnification lattice-fringe images cap-
 22 tured individual layers, smectite particles, and osmotic
 23 hydrates that lay within the depth of focus in the vitreous
 24 ice sample (estimated to be >100 nm for 80 k×
 25 magnification). These images revealed that the majority
 26 of smectite in both the untreated and treated clays had
 27 expanded beyond all crystalline hydrate states and
 28 formed osmotic hydrates, as expected for the low NaCl
 29 concentrations. All images revealed conformational
 30 disorder including heterogeneity in smectite layer
 31 spacings.

32 An image recorded from a suspension of untreated
 33 SWy-2 illustrates the tendency of the expanded smectite
 34 to form oriented, parallel stacking configurations in the
 35 osmotic hydrate state (Figure 1a). In other cases, despite
 36 the formation of pairs or triplets of parallel smectite
 37 layers, these units were rotated with respect to each
 38 other within the larger ensemble (Figure 1b). Partial
 39 osmotic hydrates that also include regions of crystalline
 40 hydrates with interlayer spacings consistent with both
 41 two- and three-water layers are shown in Figure 2.
 42 Completely delaminated individual clay layers with little
 43 evident curvature were also observed (Figure S4) as
 44 were highly disordered aggregates of layers (Figure S5).

45 The treated SWy-2 sample delaminated more com-
 46 pletely than the untreated sample following equilibration
 47 with 0.1 M NaCl solutions. More individual layers were
 48 observed and no examples of crystalline hydrates were
 49 found. As shown in Figure 3, the expanded smectite was
 50 frequently observed as parallel, stacked layers, just as
 51 observed for untreated SWy-2 suspended in 0.1 M NaCl.
 52 Fully delaminated layers, either with evident curvature
 53 or with a highly linear morphology, were observed
 54 (Figure S6). Also observed were disordered osmotic
 55 hydrates (Figure S7A) and parallel assemblies rotated
 56 relative to one another (Figure S7B), as seen for the
 57 untreated sample.

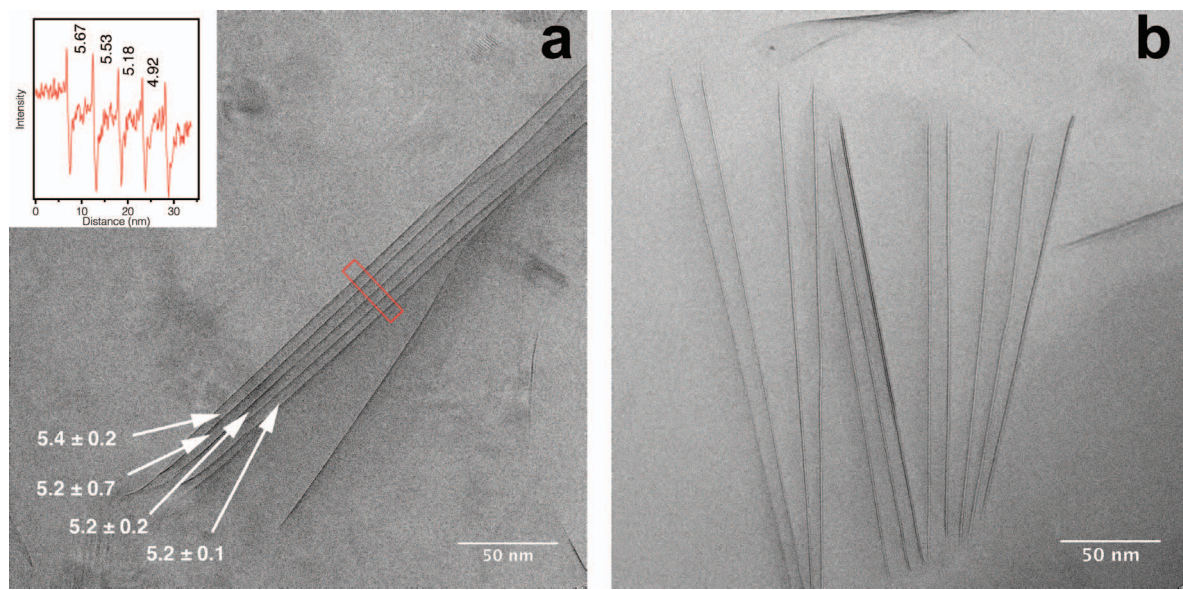


Figure 1. Cryo-TEM images of untreated SWy-2 smectite equilibrated in 0.1 M NaCl at 50 $\mu\text{g/mL}$ (a). This is an example of a more ordered stacking configuration in the osmotic hydrate state showing the average interlayer spacing and the standard deviation (nm) from five measurements along the osmotic hydrate (*cf.* Figure S9). Inset: example intensity profile from one indicated area used to determine interlayer spacing (nm). (b) Example of a partially ordered stacking configuration. The arrow indicates a pair of layers in a crystalline hydrate configuration.

As shown by the EMPA data (Table S1, deposited <http://www.clays.org/JOURNAL/JournalDeposits.html>), with the Editor in Chief and available at the long dialysis period decreased slightly the Si:Al

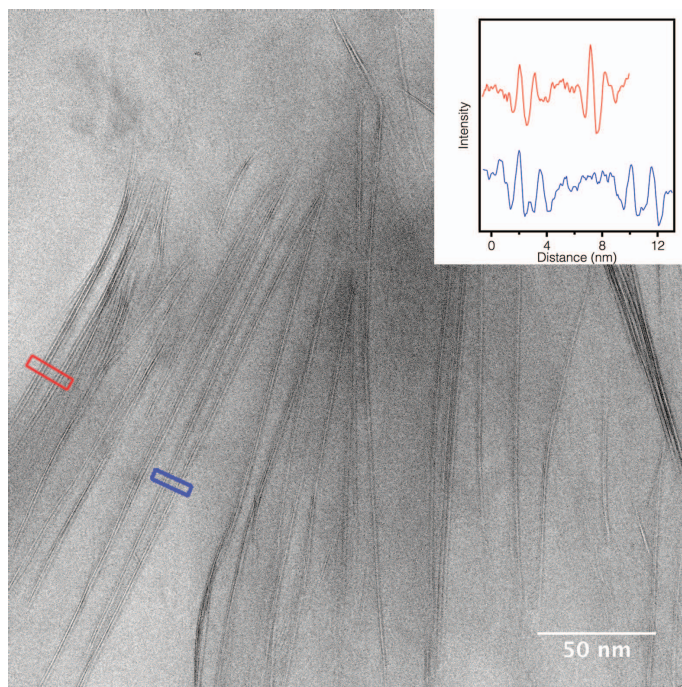


Figure 2. Cryo-TEM image of untreated SWy-2 smectite equilibrated in 0.1 M NaCl at 50 $\mu\text{g/mL}$. The image shows evidence of a partially expanded osmotic hydrate that incorporates 2- and 3-water crystalline hydrates. Inset: intensity profiles from the areas indicated reporting the interlayer spacing (nm).

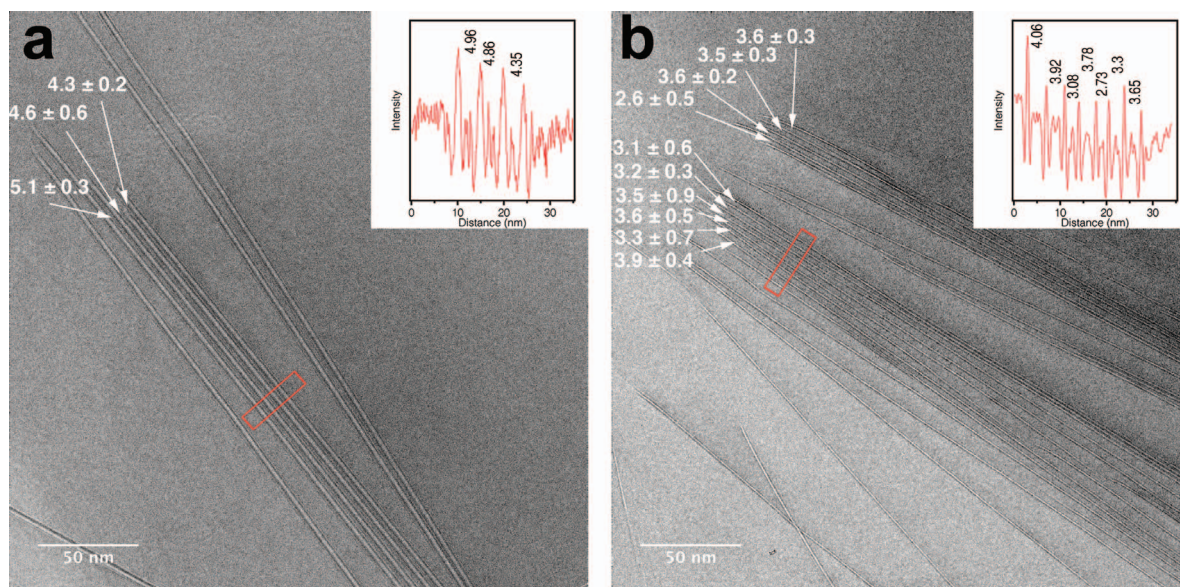


Figure 3. Cryo-TEM images of treated SWy-2 smectite equilibrated in 0.1 M NaCl at 20% w/v. Also given are the average interlayer spacing and the standard deviation (nm) from five or eight measurements along the osmotic hydrate. Insets: example intensity profiles from the regions indicated used to estimate interlayer spacing (nm).

ratio. This could be an indication of smectite dissolution and the release of Al^{3+} ions that are known to be able to displace Na^+ from the interlayer regions. Extensive release of trivalent Al ions would be expected to collapse the smectite, however, which was not observed.

For smectite particles that showed the expected osmotic hydrate structure, the interlayer spacings were measured. Because the smectite layers are oriented at an unknown tilt with respect to the image plane, such measurements could overestimate the interlayer spacing. For example, the TEM asymmetric intensity profile shown in Figure 1a probably indicates tilt of the layers. As shown in Figure S8, however, analysis of a tilt series showed that a lattice-fringe imaging condition exists only for tilt angles within $\pm 15^\circ$ or less of the beam direction. Thus, the measured spacings could be up to 5% too large.

The mean interlayer spacings from ordered osmotic hydrates are shown in Figures 1–3 as well as are the standard deviation determined from 5–8 measurements at ~ 50 -nm intervals (Figure S9). A significant range in interlayer spacings was observed, from 2.6 to 5.4 nm. Although the sample size is very small, the different clay particles in the same sample exhibited different average spacings. One plausible hypothesis is that the stoichiometric composition of the clay (and hence layer charge) was locally homogeneous but varied throughout the sample. The observations suggested an alternative hypothesis, however: the mean interlayer spacing could be a function of the number of layers in the particle if vdW interactions extend beyond a single interlayer distance. Thus, a series of numerical calculations, designed to test the idea that long-range vdW interac-

tions could significantly alter the cohesion energy of a stack of 2:1 layers, was performed.

The calculations of the vdW interactions between pairs of model 2:1 layers in an osmotic hydrate (Figure 4 inset) assumed pure water in the interlayer space because accurate dielectric functions for NaCl solutions were not available. As discussed above, the NaCl probably reduces the strength of the vdW interactions by $\sim 50\%$ relative to pure water (Marra, 1985). Because no accurate measurement of vdW shielding for saline solutions currently exists, however, no correction factor was applied to the calculations reported in Figure 4. Although the effect of salinity on the absolute magnitude or range of the vdW interaction forces is not known precisely, this uncertainty does not invalidate the calculation, which aimed to test the dependence of vdW interactions on layer number.

The calculations of layer–layer attraction, P_{vdW} , summarized in Figure 4, clearly predict that the vdW interaction forces between a pair of model clay layers in a particle are affected by the presence of additional layers. For pure water and a fixed spacing of 4 nm, the results predict that long-range interactions increase the total cohesion energy of the system by $>10\%$. Beyond ~ 5 layers, vdW interactions contribute little and, thus, can be ignored. An estimate of the electrostatic repulsion pressure, P_{EDL} , for a pair of smectite layers in 0.1 M NaCl, separated by 4 nm, is shown in Figure 4. At equilibrium, P_{vdW} and P_{EDL} should be equal and opposite. This equality is approximately satisfied if the 0.1 M NaCl shields half of the vdW contribution as indicated by the results of Marra (1985).

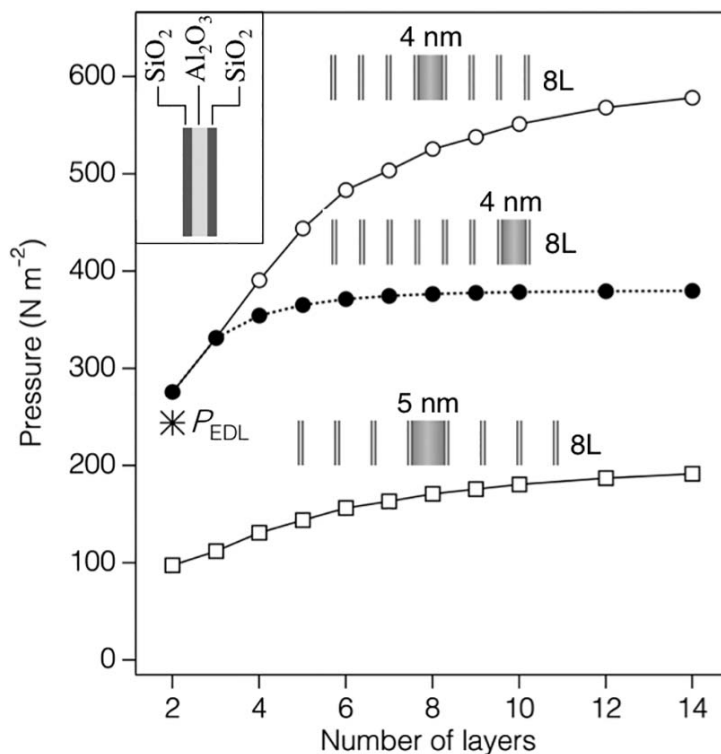


Figure 4. The calculated van der Waals force per unit area between one pair of smectite layers in water as a function of the total number of layers in a stack. A single 2:1 layer (composed of *tetrahedral-octahedral-tetrahedral* sheets), was represented by a silica-corundum-silica multilayer. (inset). Calculations were performed for the centermost (hollow symbols) and outermost (solid symbols) pair of layers and for interlayer spacings of 4 nm (circles) and 5 nm (squares). Illustrations of the geometry are depicted for 8-layer (8L) stacks, with the selected interlayer shaded. Also shown is the electrostatic repulsion pressure (P_{EDL}) calculated for a single pair of 2:1 layers with a surface potential of 250 mV at a separation of 4 nm.

The XRD data acquired from a suspension of treated SWy-2 in 0.1 M NaCl in a capillary and from a portion of the same suspension under filtration are compared in Figure 5. Under fully hydrated conditions, interlayer diffraction peaks with spacings up to 4 nm were not detectable (see figure inset). Thus, although clay particles with spacings in this range were observed at the cryo-TEM, the observed disorder broadened and weakened the scattering. Following filtration and drying, however, the clay exhibited strong (001) and (004) spacings, consistent with one water layer crystalline hydrate containing Na (Wilson *et al.*, 2004).

DISCUSSION

Smectite structure in aqueous solution

The cryo-TEM observations of lattice-fringe spacings for the hydrated smectite structure are in fair agreement with previous XRD data, supporting the present conclusion that the flash-freezing approach did not introduce artifacts. Specifically, the measured interlayer spacings, which range from 2.6 to 5.4 nm, are close to the values reported for hydrated Na-montmorillonite by Zhang *et al.* (1995) but are lower than values reported by Norrish (1954) and Amorim *et al.* (2007). The observation of

expanded smectite with a range of interlayer spacings is in agreement with prior inferences based on XRD (Pons *et al.*, 1981; Amorim *et al.*, 2007). The imaging results add considerable new insight into the structure and disorder in smectite osmotic hydrates, however.

Montmorillonite possesses a fixed negative charge in the octahedral sheet and reactive oxygen sites at layer edges that are expected to be protonated and positively charged in circumneutral solutions (Bailey, 1988; Tournassat *et al.*, 2004). These features have motivated predictions of ‘house-of-cards’ or ‘overlapping-coins’ structures (van Olphen, 1977; Jönsson *et al.*, 2008; Delhomme *et al.*, 2011). Despite the considerable disorder, no evidence was observed for such arrangements.

In the present study, smectite 2:1 layers, either in free solution or stacked in particles, typically exhibited less overall curvature (on the 100-nm and longer scale) than observed for expanded smectite imaged in epoxy (*e.g.* Schumann *et al.*, 2014). Only one image provided evidence of curvature in isolated layers (Figure S6). Flash freezing is expected to introduce fewer structural artifacts than epoxy-based sample preparations; the present observations are assumed, therefore, to depict accurately the real planarity of hydrated smectite layers. Close inspection of the images, as well as quantitative

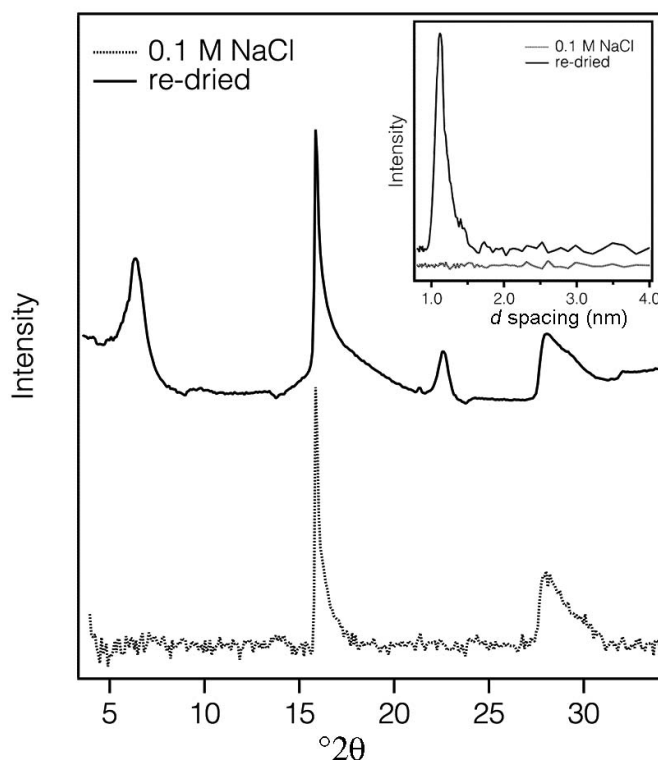


Figure 5. XRD data ($5\text{--}35^\circ 2\theta$) for treated SWy-2 smectite measured in aqueous suspension in 0.1 M NaCl (lower) and following drying (upper). Inset: low-angle scattering regions ($1.8\text{--}8^\circ 2\theta$) plotted vs. d spacing. X-ray wavelength was 1.2389 Å.

measurements of the parallelism of the ordered stacking arrangements (Figure S8), reveal fine-scale undulations in most layers. These undulations could be a consequence of metal substitutions within the layers, but higher-resolution studies will be required to explore this possibility fully.

In many images, one or more layers were observed close to, but not parallel to, layers in an ordered osmotic hydrate particle. Brownian motion is suggested here to result in osmotic hydrates that are in a state of dynamic formation and disassembly. This cannot be tested by cryo-TEM, which captures snapshots of instantaneous structure, or by conventional SAXS methods which provide measurements averaged over many particles and over a significant acquisition time. Fluid-cell TEM might allow the dynamic structure of osmotic hydrates to be observed. The present authors predict that the structural configurations observed by cryo-TEM will enable new models for scattering from disordered lamellar systems to be developed that will allow SAXS analysis of bulk solutions to provide richer and statistically more significant analysis of smectite suspensions.

Long-range attractive interactions spanning multiple smectite layers

The present calculations predict that vdW interactions spanning multiple 2:1 and water layers is a non-negligible contribution to the cohesion of expanded

smectite particles. The uncertainties in the magnitudes of the vdW forces described above do not affect this important calculation-based prediction. Long-range vdW interactions must be important in osmotic hydrates because structures with large (*i.e.* >10 nm) layer distances are stabilized. To the best of the authors' knowledge, however, no prior experimental or theoretical study of osmotic hydrates has considered the role of long-range, next-nearest-neighbor vdW interactions. This prediction may be important because it implies that the overall cohesion energy of expanded clay particles is a function of the number of layers in the particle and that the interlayer spacing will be smaller for particles with a larger number of layers. Thus, models of clay swelling based on a single pair of layers (*e.g.* Liu, 2013), or considering only next-layer interactions (*e.g.* Kleijn & Oster, 1982), will underestimate the layer-normalized cohesion energy of larger particles, and overestimate the layer distances.

Layer re-association and constraints for attachment-based crystal growth

The XRD data in Figure 5 show clearly that disordered, expanded clay layers, which exhibit no detectable 001 scattering, re-aggregate readily when the water activity is reduced by drying to form ordered crystalline hydrates with strong diffraction perpendicular to the layer plane. Because transformation of osmotic to

crystalline hydrates involves assembly of individual smectite 2:1 layers in solution, it can be classified as an example of oriented attachment-based crystal growth (OA) (Penn and Banfield, 1998). Such OA has been reported as a crystal-growth mechanism for many poorly soluble nanoparticulate minerals, including oxides and sulfides (Penn *et al.*, 2001; Huang *et al.*, 2003), and has been observed in suspensions of nanoparticles with a range of morphologies (Yuwono *et al.*, 2010; Frandsen *et al.*, 2014). The case of assembly of 2:1 smectite layers is distinct from other growth processes described as OA because the attachment process is readily reversible due to the unusually low strength of layer–layer interactions (because attachment does not involve the formation of covalent or ionic bonds). The authors here do not mean to imply that smectite particles form originally through the stacking of individual 2:1 layers that nucleate homogeneously in solution (although this sometimes may be the case). Rather, the 2:1 layer assembly is described as one of the steps in the dynamic process of swelling, disaggregation, and re-aggregation that probably occurs innumerable times over the ‘lifetime’ of smectite particles.

In research on OA-based crystal growth, the nature of nanoparticle interactions in aqueous solution and the distances over which they interact are uncertain. *In situ* fluid-cell TEM observations of OA-based crystal growth of ferrihydrite indicate the operation of long-range particle-particle interactions (Li *et al.*, 2012). Studies of smectite swelling and restacking can provide insights into interparticle forces involved in OA-based crystal growth because the two-dimensional geometry enables interactions that are parallel and normal to the 2:1 layers to be resolved. Observations of attractive forces in the 3 to >20 nm range in expanded clays indicate that particle–particle interactions can occur over such distances (although nanoparticle size and morphology will affect interaction distances).

In OA-based growth, an orienting force is suspected to align nanoparticles as they approach so that interface elimination can yield a single crystal (Li *et al.*, 2012; Zhang and Banfield, 2014). Cryo-TEM images show that separated smectite layers in ordered particles are parallel to each other. This geometry is explained conceptually by DLVO theory in which the balance between attractive and repulsive forces orients the surfaces. The cryo-TEM data also show that layers tend to overlap each other. This implies that lateral forces parallel to the 2:1 layers in the osmotic hydrate are sufficiently strong to drive the system to an energy minimum in which the layers superimpose. Attractive layer–layer vdW forces could provide the driving force for this alignment, although electrostatic forces must play a role once the layers are close enough that the electrical double layers overlap. Cryo-TEM observations of smectite *in aqua*, thus, provide insight into the nature of layer–layer interactions controlling clay expansion and restacking and can

inform an understanding of related colloidal phenomena including OA-based crystal growth.

CONCLUSIONS

Cryo-TEM observations of flash-frozen suspensions of smectite in 0.1 M NaCl solution revealed that osmotic hydrates, composed of highly planar and close to parallel 2:1 layers, coexisted with 2:1 layers in a range of disordered conformations, but without evidence of alternative edge-to-sheet interactions. The large range of interlayer spacings measured in the osmotic hydrates suggested a role for long-range attractive van der Waals interactions in determining equilibrium structure. Calculations of van der Waals forces in a multi-layer model of expanded smectite predicted that attractive forces acting over at least four smectite interlayers will influence osmotic hydrate cohesion energy. Due to the disorder in the expanded state, (001) diffraction peaks were not detectable in XRD data, but were observed following restacking (through drying). Assembly of individual smectite 2:1 layers in solution can be classified as an example of oriented attachment-based (OA) crystal growth. Further elucidation of the forces that act to align smectite particles during stacking, aided by cryo-TEM observations, will improve understanding of both clay swelling and OA based growth.

ACKNOWLEDGMENTS

The authors thank Sean Mulcahy for performing electron beam microprobe analysis and Dr Roger French for access to and assistance with the *Gecko Hamaker* code. This work was supported by the Office of Science, Office of Basic Energy Sciences (BES), Chemical Sciences, Geosciences, and Biosciences Division, of the U.S. Department of Energy (DOE) under Contract No. DE-AC02-05CH11231. RMT was supported by the U.S. Department of Energy Used Fuel Disposition (UFD) Campaign, Contract No. DE-AC02-05CH11231. The *Gecko Hamaker* code was developed with support from DOE BES Materials Science and Engineering Division, Biomolecular Materials (BMM) under award DE-SC0008068.

REFERENCES

- Amorim, C.L.G., Lopes, C.L.G., Barroso, R.C., Queiroz, J.C., Alves, D.B., Perez, C.A., and Schelin, H.R. (2007) Effect of clay–water interactions on clay swelling by X-ray diffraction. *Nuclear Instruments and Methods in Physics Research A*, **580**, 768–770.
- Anderson, R.L., Ratcliffe, I., Greenwell, H.C., Williams, P.A., Cliffe, S., and Coveney, P.V. (2010) Clay swelling – a challenge in the oilfield. *Earth-Science Reviews*, **98**, 201–216.
- Bailey, S.W. (1988) *Hydrous Phyllosilicates (exclusive of Micas)*. Reviews in Mineralogy, **19**, Mineralogical Society of America, Washington, D.C.
- Cheng, Y. (2015) Single-particle cryo-EM at crystallographic resolution. *Cell*, **161**, 450–457.
- Comolli, L.R., Luef, B., and Chan, C.S. (2011) High-resolution 2D and 3D cryo-TEM reveals structural adaptations of two

- stalk-forming bacteria to an Fe-oxidizing lifestyle. *Environmental Microbiology*, **13**, 2915–2929.
- Davies, B. and Ninham, B.W. (1972) Van der Waals forces in electrolytes. *Journal of Chemical Physics*, **56**, 5792–5801.
- Dazas, B., Lanson, B., Delville, A., Robert, J.L., Komarneni, S., Michot, L.J., and Ferrage, E. (2015) *Journal of Physical Chemistry C*, **119**, 4158–4172.
- Delhorme, M., Jönsson, B., and Labbez, C. (2011) Monte Carlo simulations of a clay inspired model suspension: The role of rim charge. *Soft Matter*, **8**, 9691–9704.
- Faisandier, K., Pons, C.H., Tchoubar, D., and Thomas, F. (1998) Structural organization of Na- and K-montmorillonite suspensions in response to osmotic and thermal stresses. *Clays and Clay Minerals*, **46**, 636–648.
- Ferrage, E., Lanson, B., Sakharov, B.A., and Drits, V.A. (2005) Investigation of smectite hydration properties by modeling experimental X-ray diffraction patterns: Part I. Montmorillonite hydration properties. *American Mineralogist*, **90**, 1358–1374.
- Foster, M.D. (1955) The relation between composition and swelling in clays. *Clays and Clay Minerals*, **3**, 205–220.
- Frandsen, C., Legg, B., Comolli, L.R., Zhang, H., Gilbert, B., Johnson, E., and Banfield, J.F. (2014) Aggregation-induced growth and transformation of β -FeOOH nanorods to micron-sized α -Fe₂O₃ spindles. *CrystEngComm*, **16**, 1451–1458.
- French, R.H., Müllejans, H., and Jones, D.J. (1998) Optical properties of aluminum oxide: determined from vacuum ultraviolet and electron energy-loss spectroscopies. *Journal of the American Ceramic Society*, **81**, 2549–2557.
- Greathouse, J.A., Feller, S.E., and McQuarrie, D. (1994) The modified Gouy-Chapman theory: comparisons between electrical double layer models of clay swelling. *Langmuir*, **10**, 2125–2130.
- Grodzinsky, A.J. (2011) *Fields, Forces, and Flows in Biological Systems*. Garland Science
- Guthrie, G.D. and Veblen, D.R. (1989) High-resolution transmission electron microscopy of mixed-layer illite/smectite: Computer simulations. *Clays and Clay Minerals*, **37**, 1–11.
- Hou, J., Li, H., and Zhu, H. (2009) Determination of clay surface potential: A more reliable approach. *Soil Science Society of America Journal*, **73**, 1658–1663.
- Huang, F., Zhang, H.Z., and Banfield, J.F. (2003) The role of oriented attachment crystal growth in hydrothermal coarsening of nanocrystalline ZnS. *Journal of Physical Chemistry B*, **107**, 10470–10475.
- Jönsson, B., Labbez, C., and Cabane, B. (2008) Interaction of nanometric clay platelets. *Langmuir*, **24**, 11406–11413.
- Klein, W.B. and Oster, J.D. (1982) A model of clay swelling and tactoid formation. *Clays and Clay Minerals*, **30**, 383–390.
- Laird, D.A. (2006) Influence of layer charge on swelling of smectites. *Applied Clay Science*, **34**, 74–87.
- Legg, B., Zhu, M., Comolli, L.R., Gilbert, B., and Banfield, J.F. (2014) Determination of the three-dimensional structure of ferrihydrite nanoparticle aggregates. *Langmuir*, **30**, 9931–9940.
- Li, D., Nielsen, M.H., Lee, J.R.I., Frandsen, C., Banfield, J.F., and De Yoreo, J.J. (2012) Direction-specific interactions control crystal growth by oriented attachment. *Science*, **336**, 1014–1018.
- Lifshitz, E.M. (1956) The theory of molecular attractive forces between solids. *Soviet Physics* **2**, 73–83.
- Liu, L. (2013) Prediction of swelling pressures of different types of bentonite in dilute solutions. *Colloids and Surfaces A*, **343**, 303–318.
- Low, P.F. and Margheim, J.F. (1979) Swelling of clay. 1. Basic concepts and empirical equations. *Soil Science Society of America Journal*, **43**, 473–481.
- Luckham, P.F. and Rossi, S. (1999) The colloidal and rheological properties of bentonite. *Advances in Colloidal Science*, **82**, 43–92.
- Luef, B., Fakra, S.C., Csencsits, R., Wrighton, K.C., Williams, K.H., Wilkins, M.J., Downing, K.H., Long, P.E., Comolli, L.R., and Banfield, J.F. (2012) Iron-reducing bacteria accumulate ferric oxyhydroxide nanoparticle aggregates that may support planktonic growth. *ISME Journal*, **2012**, 1–13.
- Marra, J. (1985) Direct measurements of attractive van der Waals and adhesion forces between uncharged lipid bilayers in aqueous solutions. *Journal of Colloid and Interface Science*, **109**, 11–20.
- Miller, S.E. and Low, P.F. (1990) Characterization of the electrical double layer of montmorillonite. *Langmuir*, **6**, 572–578.
- Missanna, T. and Adell, A. (2000) On the applicability of DLVO theory to the prediction of clay colloids stability. *Journal of Colloid and Interface Science*, **230**, 150–156.
- Norrish, K. (1954) Manner of swelling of montmorillonite. *Nature*, **173**, 256–257.
- Paineau, E., Bihannic, I., Baravian, C., Philippe, A.-M., Davidson, P., Levitz, P., Funari, S.S., Rochas, C., and Michot, L.J. (2011) Aqueous suspensions of natural swelling clay minerals. 1. Structure and electrostatic interactions. *Langmuir*, **27**, 5562–5573.
- Parsegian, V.A. (2006) *Van der Waals Forces*. Cambridge University Press, Cambridge, UK.
- Penn, R.L. and Banfield, J.F. (1998) Imperfect oriented attachment: Dislocation generation in defect-free nanocrystals. *Science*, **281**, 969–971.
- Penn, R.L., Oskam, G., Strathmann, T.J., Searson, P.C., Stone, A.T., and Veblen, D.R. (2001) Epitaxial assembly in aged colloids. *Journal of Physical Chemistry B*, **105**, 2177–2182.
- Podgornik, R. and Parsegian, V.A. (2004) Van der Waals interactions across stratified media. *Journal of Chemical Physics*, **120**, 3401–3405.
- Pons, C.H., Rousseaux, F., and Tchoubar, D. (1981) Utilisation du rayonnement synchrotron en diffusion aux petits angles pour l'étude du gonflement des smectites: I. Etude du système eau-montmorillonite-Na en fonction de la température. *Clay Minerals*, **16**, 23–42.
- Quirk, J.P. and Marčelja, S. (1997) Application of double-layer theories to the extensive crystalline swelling of Li-montmorillonite. *Langmuir*, **13**, 6241–6248.
- Rajter, R.F., French, R.H., Ching, W.Y., Podgornik, R., and Parsegian, A.V. (2013) Chirality-dependent properties of carbon nanotubes: electronic structure, optical dispersion properties, Hamaker coefficients and van der Waals–London dispersion interactions. *RSC Advances*, **3**, 823–842.
- Schuman, D., Hesse, R., Sears, S.K., and Vali, H. (2014) Expansion behavior of octadecylammonium-exchanged low-to high-charge reference smectite-group minerals as revealed by high-resolution transmission electron microscopy on ultrathin sections. *Clays and Clay Minerals*, **62**, 336–353.
- Schuman, D., Hesse, R., Sears, S.K., and Vali, H. (2014) Expansion behavior of octadecylammonium-exchanged low-to high-charge reference smectite-group minerals as revealed by high-resolution transmission electron microscopy on ultrathin sections. *Clays and Clay Minerals*, **62**, 336–353.
- Segad, M., Hanski, S., Olsson, U., Ruokolainen, J., Akesson, T., and Jonsson, B. (2012) Microstructural and swelling properties of Ca and Na montmorillonite: (*in situ*) observations with cryo-TEM and SAXS. *Journal of Physical Chemistry C*, **116**, 7596–7601.
- Slade, P.G., Quirk, J.P., and Norrish, K. (1991) Crystalline swelling of smectite samples in concentrated NaCl solutions in relation to layer charge. *Clays and Clay Minerals*, **39**, 1

- 234–238.
- 1 Svensson, P.D. and Hansen, S. (2013) Combined salt and
2 temperature impact on montmorillonite hydration. *Clays
3 and Clay Minerals*, **61**, 328–341.
- 4 Tan, G.L., Lemon, M.F., Jones, D.J., and French, R.H. (2005)
5 Optical properties and London dispersion interaction of
6 amorphous and crystalline SiO₂ determined by vacuum
7 ultraviolet spectroscopy and spectroscopic ellipsometry.
8 *Physical Review B* **72**, 205117.
- 9 Tournassat, C., Ferrage, E., Poinssignon, C., and Charlet, L.
10 (2004) The titration of clay minerals II. Structure-based
11 model and implications for clay reactivity. *Journal of
12 Colloid and Interface Science*, **273**, 234–246.
- 13 van Olphen, H. (1977) *An Introduction to Clay Colloid
14 Chemistry*. Interscience Publishers, New York.
- 15 Viani, B.E., Low, P.F., and Roth, C.B. (1983) Direct
16 measurement of the relation between interlayer force and
17 interlayer distance in the swelling of montmorillonite.
18 *Journal of Colloid and Interface Science*, **96**, 229–244.
- 19 Wilson, J., Cuadros, J., and Cressey, G. (2004) An *in situ* time-
20 resolved XRD-PSD investigation into Na-montmorillonite
21 interlayer and particle rearrangement during dehydration. *Clays
22 and Clay Minerals*, **52**, 180–191.
- 23 Yuwono, V.M., Burrows, N.D., Soltis, J.A., and Penn, R.L.
24 (2010) Oriented aggregation: Formation and transformation
25 of mesocrystal intermediates revealed. *Journal of the
26 American Chemical Society*, **132**, 2163–2165.
- 27 Zhang, F., Zhang, Z.Z., Low, P.F., and Roth, C.B. (1993) The
28 effect of temperature on the swelling of montmorillonite.
29 *Clay Minerals*, **28**, 25–31.
- 30 Zhang, F.S., Low, P.F., and Roth, C.B. (1995) Effects of
31 monovalent, exchangeable cations and electrolytes on the
32 relation between swelling pressure and interlayer distance in
33 montmorillonite. *Journal of Colloid and Interface Science*,
34 **173**, 34–41.
- 35 Zhang, H. and Banfield, J.F. (2014) Interatomic Coulombic
36 interactions as the driving force for oriented attachment.
37 *CrystEngComm*, **16**, 1568–1578.
- 38
39
40
41
42
43
44
45
46
47
48
49
50
51
52
53
54
55
56
57
- (Received 24 February 2015; revised 15 January 2016;
Ms. 964; AE: M.A. Velbel)